Improved Electrophile Design for Exquisite Covalent Molecule Selectivity

José L. Montaño, Brian J. Wang, Regan F. Volk, Virginia G. Garda, Balyn W. Zaro*

Department of Pharmaceutical Chemistry and Cardiovascular Research Institute University, University of California, San Francisco, CA 94305.

KEYWORDS: covalent inhibitor, chemical proteomics, drug development, drug selectivity

ABSTRACT: Covalent inhibitors continue to show therapeutic promise. However, off-target reactivity challenges the field. Extensive efforts have been exerted to solve this issue by varying the reactivity attributes of electrophilic warheads, with features such as reversibility or metabolic vulnerability. Here we report the development of a new approach to increase the selectivity of covalent probes and small molecule inhibitors that is independent of warhead reactivity features and can be used in concert with already-existing methods. Using the Bruton's Tyrosine Kinase (BTK) inhibitor Ibrutinib scaffold for our proof-of-concept, we reasoned that increasing the steric bulk of fumarate-based electrophiles on Ibrutinib should improve selectivity via the steric exclusion of off-targets but ideally retain rates of cysteine reactivity comparable to that of an acrylamide. Using chemical proteomic techniques, we demonstrate that elaboration of the electrophile to a *tert*-Butyl (*t*-Bu) fumarate ester significantly decreases time-dependent off-target reactivity and abolishes time-independent off-target reactivity but retains BTK target engagement. While an alkyne-bearing probe analog of Ibrutinib has 247 protein targets, our *t*-Bu fumarate Ibrutinib probe analog has only 7 protein targets. Of these 7 targets, BTK is the only time-independent target. This 2-order-of-magnitude increase in selectivity is also conferred to the t-Bu inhibitor itself. By shotgun proteomics, we investigated the consequences of treatment with Ibrutinib and our *t*-Bu analog and discovered that only 8 proteins are downregulated in response to treatment with the *t*-Bu analog compared to 107 with Ibrutinib. Of these 8 proteins, 7 are also downregulated by Ibrutinib and a majority of these targets are associated with BTK biology. Taken together, these findings reveal a previously-unappreciated opportunity to increase cysteine-reactive covalent inhibitor selectivity through electrophilic structure optimization.

INTRODUCTION

Irreversible covalent molecules have long been explored as therapeutics in human disease. Their irreversible mechanism of action (MoA) is believed to i) minimize the risk of treatment-acquired mutations which can lead to drug-resistance and ii) lower both the dose and frequency of drug administration.[1] However, the very same characteristic that has endowed these molecules with these attractive features has also elicited much skepticism in their potential to be safe and viable long-term therapeutics. Mainly, much like the target engagement of their intended target, any off-targets of irreversible inhibitors may also be engaged irreversibly. Nonetheless, there are currently over 40 covalent inhibitors approved by the FDA for the treatment of several clinical indications, including cancer.[2] The success of these drugs in the clinic likely stems from careful structure-activity relationship (SAR) studies that yield highly selective inhibitors and, in some instances, clever exploitation of unique nucleophilic residues on proteins (i.e. cysteines on kinases) which may further improve the molecule's selectivity across the proteome. Despite the clinical success, recent advances in chemical proteomic methods have revealed the off-target promiscuity of these covalent kinase inhibitors extends to both kinase and non-kinase proteins. Critically, this off-target reactivity may be associated with target-independent cytotoxicity. Much of this off-target reactivity is time-dependent, meaning that while initially these inhibitors are quite selective for their intended target, they begin to engage off-targets over time.[3]

Many creative approaches have been applied to solve this problem, a majority of which have used the Bruton's tyrosine kinase (BTK) inhibitor Ibrutinib for proof-of-concept. The design of covalent reversible inhibitors has emerged as a viable strategy, demonstrating improved selectivity by engaging on-targets more durably compared to off-targets.[4–6] Covalent reactive groups ('warheads') with tunable reactivity have also been applied successful in developing more selective covalent inhibitors.[7,8] The use of hetero α-substituted methacrylamide-based electrophiles has recently been shown to endow inhibitors with reduced reactivity and increased selectivity relative to the acrylamide counterpart.[9] Additionally, we have previously shown that the use of metabolically labile warheads can result in inhibitors with kinetic-selectivity and decreased time-dependent off-target engagement events.[10] In this approach, the acrylamide (Michael acceptor) of Ibrutinib was replaced with a methyl fumarate. This yielded a highly reactive warhead that engages BTK at a much faster rate than its inactivation by human carboxylesterase 1 (hCES1), but reduces time-dependent off-target engagement. However, in the absence of hCES1, the methyl fumarate analogue probe of Ibrutinib has increased free-cysteine reactivity and significantly higher-background labelling compared to the parent Ibrutinib probe.

Previously solved crystal structures of Ibrutinib covalently bound to Cys481 of BTK indicate the presence of available space for the elaboration of electrophiles appended to the Ibrutinib scaffold.11 This prompted us to ask if the presence of this cavity would allow inhibitors with bulkier electrophiles to retain BTK engagement, while reducing off-targets via steric exclusion. Although fumarate-based warheads can be easilyderivatized to yield electrophiles with varying levels of steric bulk, the ester substituent of fumarates can drastically alter the overall reactivity of the αβ-unsaturated carbonyl. Therefore, we wondered if we could develop Ibrutinib analogues containing fumarate-based warheads that are i) relatively sterically bulky and ii) as cysteine reactive as the acrylamide on Ibrutinib.

RESULTS

We developed a small library of fumarate analogues of Ibrutinib (**1**), each with increasing bulk and varying levels of electron donating properties (Figure 1a). To assess the overall reactivity of inhibitors **1-4**, we carried out a cysteine reactivity assay. The *tert*-Butyl fumarate (*t*-Bu) analogue (**3**) possesses a reactivity comparable to that of the acrylamide parent compound (**1**) (28.69 ± 2.18 L mol^{-1} min^{-1} and 17.81 ± 1.88 L mol^{-1} min^{-1}, respectively), while **2** and **4** has significantly greater reactivity towards free reduced cysteine (Figure 1b). Intrigued by these results, we then asked if **3** was still capable of engaging BTK despite its increased bulk at the electrophilic moiety. We further modified Ibrutinib (**1**) and its fumarate ester analogues (**2-4**) with alkyne handles to yield probes **5-8** (Figure 1a).

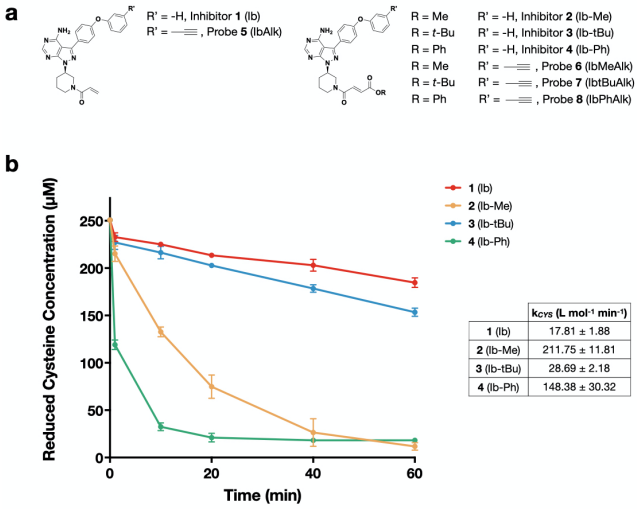

Figure 1. Design and initial cysteine reactivity assessment of fumarate-based Ibrutinib analogues. (a) Structures of inhibitors and probes used in this study. (b) Comparison of the reactivity of **1**-**4** *in vitro* in a cysteine binding assay using Ellman's reagent. Whereas the reactivity of **1** and **3** were comparable, the free reduced cysteine levels were more rapidly decreased in the presence of **2** and **4**. The second-order rate constants were calculated and are presented in the table to the right.

To qualitatively compare global reactivity profiles and assess BTK target engagement of **5-8**, we took advantage of established gel-based chemical probe labeling techniques.13,14 Whole Mino cells were subjected to increasing concentrations of probe (**5-8**; 1 nM – 1 μM, 16 h) prior to lysis and conjugation of TAMRA-azide via copper(I)-catalyzed azide-alkyne cycloaddition (CuAAC) followed by SDS-PAGE and in-gel fluorescence scanning. Remarkably, while probes **5**, **6**, and **8** began showing significant off-target activity at 1 μM, probe **7** remained highly selective for BTK (Figure 2a). Since it is known that many covalent drugs, including Ibrutinib, have time-dependent off-target activity2,15, we next tested the time-dependent labelling of proteins by probes **5-8** (1 μM, 1 – 24 h). After 1 hour, each probe, with the exception of **8**, appeared to engage BTK selectively. However, by 8 hours, all probes with the exception of **7**, began to qualitatively display time-dependent promiscuity (Figure 2b).

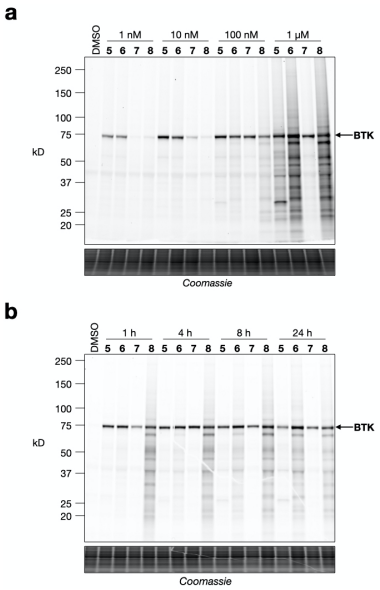

Figure 2. In-gel characterization of global protein labelling by fumarate-based Ibrutinib probes. (a) In-gel fluorescence scanning data for concentration-dependent (1 nM - 1 μM ; 16 h) and (b) time-dependent (1 h - 24 h ; 1 μM) labelling of proteins in whole Mino cells by probes **5**-**8**. In both cases, TAMRA-azide was conjugated onto labelled protein via CuAAC prior to SDS-PAGE

With what appeared to be a highly selective probe for BTK in hand, we went on to compare protein targets of the original Ibrutinib probe (**5**, IbAlk) and the new *t*-Bu probe (**7**, IbtBuAlk) using comparative MS-based chemical proteomics techniques. To generate a list of true probe targets for **5** and **7**, isotopically-labelled 'heavy' or 'light' cultures of Mino cells were treated with probe (**5** or **7;** 1 μM, 24 h) or no probe (DMSO), respectively, prior to lysis and 1:1 mixing of heavy/light (probe/no probe) lysate pairs. Proteins covalently engaged by probe were enriched via biotin-azide CuAAC conjugation followed by streptavidin enrichment, tryptic digest and LC-MS analysis (Figure S1, Tables S1 and S2). In this approach, proteins preferentially enriched by a probe are identified by having a characteristic probe versus (vs) DMSO vehicle SILAC enrichment ratio of ≥ 2. While we were able to identify only 7 true targets of probe **7**, we identified 247 targets for probe **5** (Tables S3 and S4). Notably, all 7 targets of probe **7**, including BTK, are also shared with probe **5** (Figure 3a).

Previous reports by ourselves and others have highlighted the time-dependent and -independent protein targets of covalent inhibitors and probes. Therefore, we were curious to see if probe **7** would also have a similar distinction between targets. We performed comparative MS-based time course experiments, where

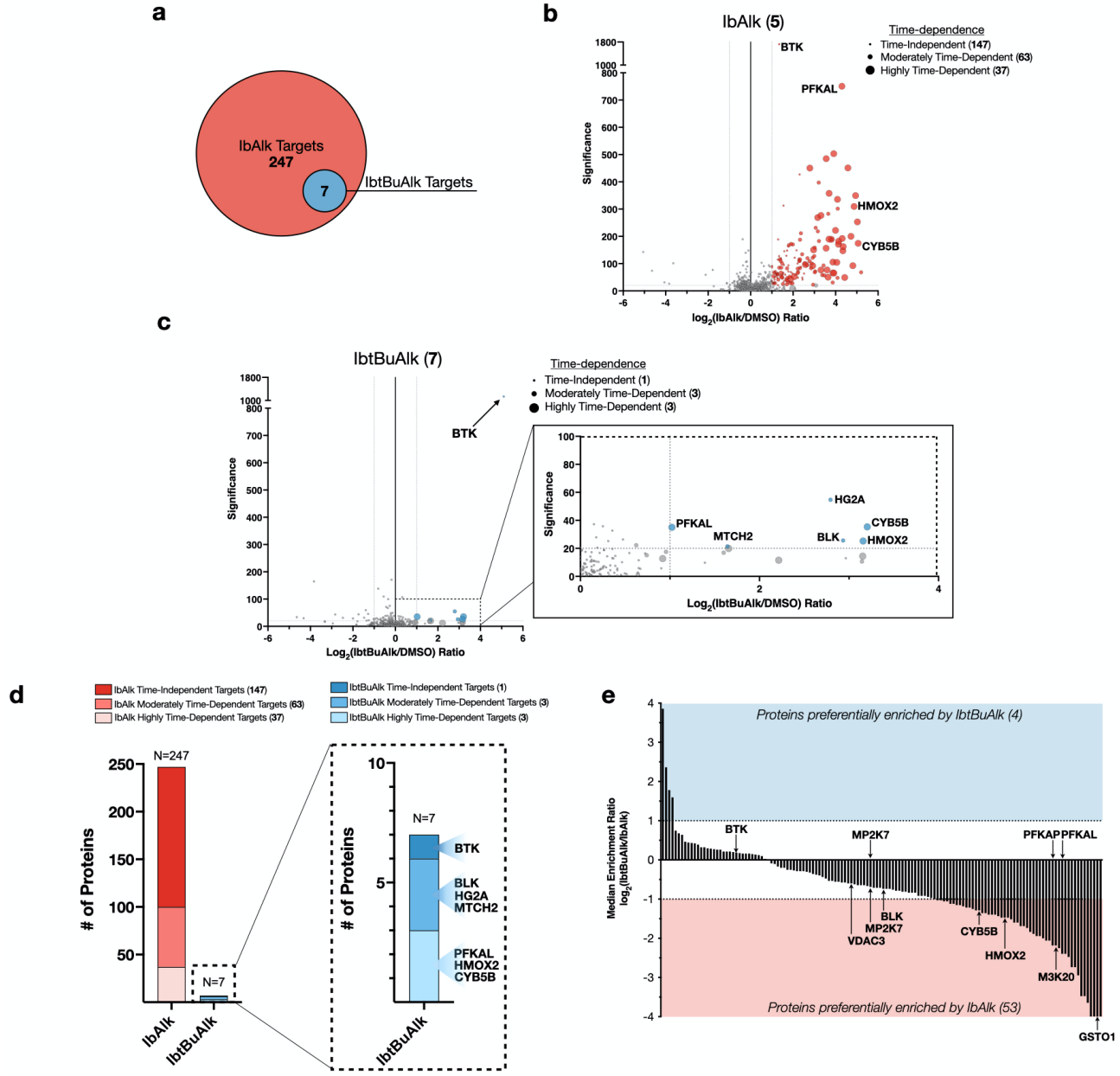

Figure 3. SILAC-based quantitative proteomic analysis of IbAlk and IbtBuAlk protein targets. (a) Probe vs no probe SILAC analysis identified a total of 247 targets of IbAlk (**5**) and 7 targets for IbtBuAlk (**7**). All 7 protein targets of IbtBuAlk were also found to be targets of IbAlk. (b) Volcano plot of proteins enriched by IbAlk and (c) IbtBuAlk from SILAC-ABPP probe vs no probe experiments. Size of bubbles indicates whether a protein target is either i) time-independent, ii) moderately time-dependent, or iii) highly time-dependent as determined from separate SILAC-ABPP 1 h vs 24 h experiments. (d) Bar graphs showing the total protein targets for each probe and their time-dependence. Of the 7 protein targets of IbtBuAlk, the only time-independent target was BTK. (e) Waterfall plot of proteins preferentially enriched by either IbtBuAlk or IbAlk in SILAC-ABPP probe vs probe experiments.

isotopically labelled Mino cells were dosed with probe (**5** or **7**; 1 μM) for either 1 hour or 24 hours (Figure S1). An enrichment ratio was generated comparing probe enrichment following 24 h of probe treatment compared to 1h of probe treatment (24 h/1 h) (Tables S5 and S6). We binned time-dependence for true targets of each probe into 3 categories: i) time-independent (Enrichment Ratio 24 h vs 1 h < 2), ii) moderately time-dependent (Enrichment Ratio 24h vs 1 h $2 \leq X < 4$) and iii) highly time-dependent (Enrichment Ratio 24h vs 1h ≥ 4) (Figures 3b and 3c, Figures S3a and S3b). Importantly, enrichment of BTK between 1 hour and 24 hours was unchanged (enrichment ratio ~1) for both **5** and **7**, indicating saturated target engagement of BTK by both probes within 1 h of treatment. However, while **5** had over 100 time-dependent targets, **7** had only 6 (Figure 3d, Figure S3c). Strikingly, BTK was the only time-independent target of **7**.

To directly compare the reactivity of **5** and **7** over 24 hours, probe vs probe comparative SILAC studies were performed (Figure S1). Isotopically heavy or light Mino cells were treated with indicated probe (**5** or **7**; 1 μM). While BTK enrichment

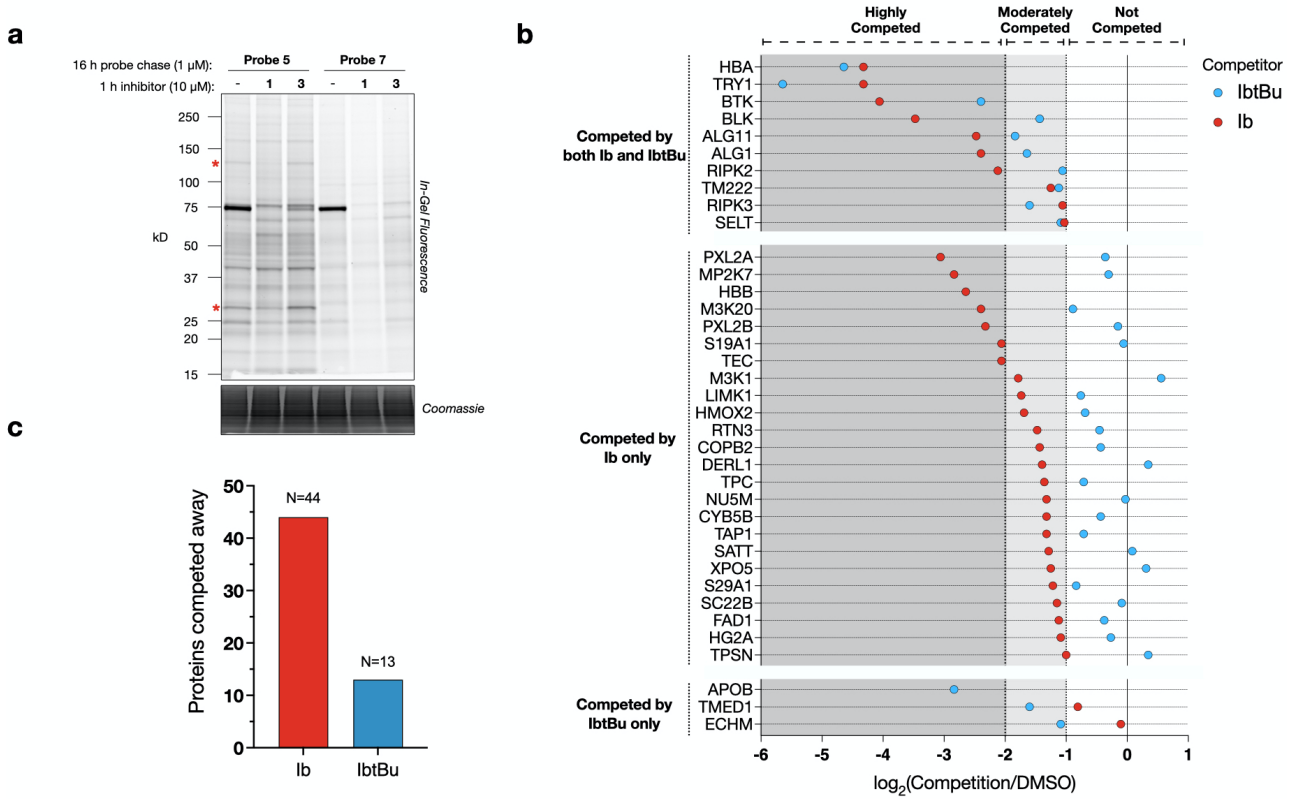

Figure 4. Characterization of proteins competed away by pre-treatment with Ibrutinib and IbtBu inhibitors. (a) Gel-based competitive ABPP showing differences in protein enrichment profile in Mino cells pre-treated with either DMSO, Ibrutinib (1) or IbtBu (3) for 1 hour at 10 uM and chased with either IbAlk (5) (lanes 1-3) or IbtBuAlk (7) (lanes 4-6). The dark band at about 75 kD is BTK. (b) Plot showing proteins competed away by i) both Ib and IbtBu, ii) only Ib and iii) only IbtBu in competition probe labelling SILAC experiments. Ratios from both Ib (red circles) and IbtBu (blue circles) competition are plotted for each protein. Proteins which appeared to be competed were also required to have a significance value of ≥ 20 ($p \leq 0.01$). (c) Bar graph comparing the total number of proteins competed away by competition with either Ibrutinib or IbtBu as determined by probe labelling SILAC experiments.

was comparable for both probes following 24 hour treatment, global reactivity of **5** was markedly higher with 53 proteins preferentially enriched by **5** compared to 4 by **7** (Figure 3e, Figure S4, Table S7). Known off-targets of both probes such as PFKAL, CYB5B, and HMOX2 were each preferentially enriched by **5** (Figure 3e).

Having confirmed that **7** was more selective for BTK than **5** in a time-dependent and -independent manner, we next asked if this increase in selectivity was conferred by the inhibitor. For gel-based competitive probe experiments, Mino cells were pre-treated with either DMSO or inhibitor (**1** or **3**; 10 μM, 1 h). Following pre-treatment, the indicated probe was added (**5** or **7**; 1 μM, 16 h) prior to downstream processing for in-gel fluorescence scanning. While both inhibitors competed away BTK probe labeling, we noticed that some bands labeled by **5** were competed by **1** and not **3,** examples of which are denoted with red asterisks (Figure 4a).

We complemented these competitive gel-based experiments with MS-based studies. We binned probe **5** targets as i) non-competed (enrichment ratio > 0.5), ii) moderately competed (enrichment ratio $0.25 < X \leq 0.5$), or iii) highly competed (enrichment ratio ≤ 0.25) (Figure 4b, Tables S8 and S9). BTK target engagement by **3** was comparable to that of **1** in competing away labeling by **5**. In total, 10 protein targets were competed by pre-treatment with both **1** and **3** (Figure 4b). There was also a large subset of proteins engaged by **1** and not by **3**, while only 3 proteins were uniquely competed by **3**. In total, **1** competed 44 targets compared to 13 by **3** (Figure 4c, Figure S5a and S5b). Taken together, these results indicate that the *t*-Bu fumarate ester analogue is exceptionally selective for BTK.

Given the differences in reactivity between our *t*-Bu fumarate-bearing compound and the parent acrylamide compound, we wondered if the proteomic consequences of inhibitor treatment would differ. To that end, Mino cells were treated with **1**, **3** or DMSO control (1 μM, 48 h) and processed for shotgun whole protein MS analysis. Using label-free quantification methods we identified approximately 3500 proteins across each dataset run in biological and technical duplicate, a subset of which were down-regulated in response to inhibitor treatment compared to DMSO (≥ 2-fold change, Figure 5a and 5b). Treatment with **1** resulted in the downregulation of 107 proteins compared to only 8 proteins when cells were treated with **3** (Figure 5a and 5b, Tables S10 and S11). Of the 8 proteins downregulated upon treatment with **3**, 7 were also downregulated by **1** (Figure 5c). Of these 7 overlapping proteins, 5 are implicated in B-cell receptor signaling (Figure 5c).16–23

Finally, we asked if these differences in promiscuity would alter cytotoxicity profiles. Mino cells were treated with **1** or **3** at increasing concentrations for 48 h. Cell viability assays revealed differing toxicity profiles between both inhibitors

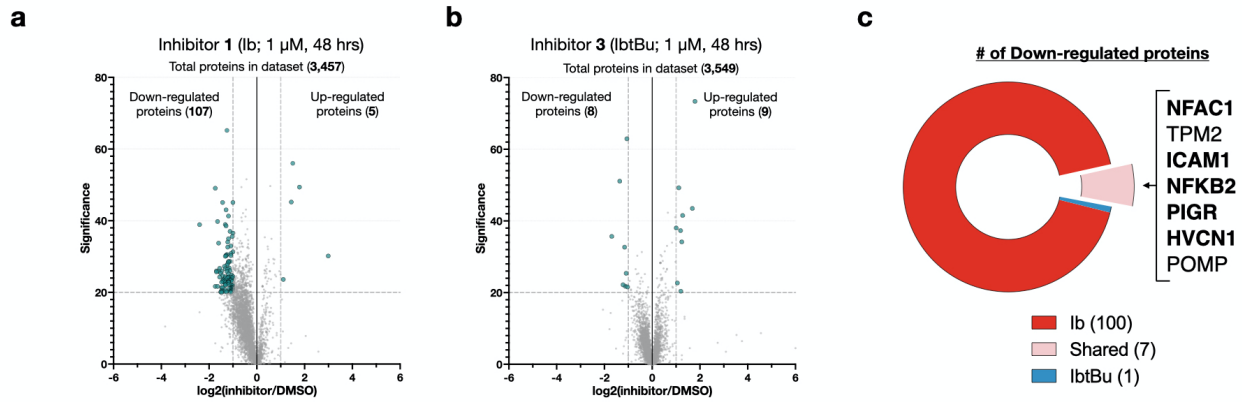

Figure 5. Assessment of global proteome changes in inhibitor treated Mino cells. (a) Volcano plot showing the changes in protein expression levels as a result of treatment with inhibitor 1 (Ib; 1 μM, 48 h) or (b) inhibitor 3 (IbtBu; 1 μM, 48 h). Values are all relative to DMSO control treated cells. (c) Breakdown of the down-regulated proteins in both Ib and IbtBu treated Mino cells. While Ib treatment resulted in the down-regulation of 107 proteins, treatment with IbtBu resulted in the down-regulation of only 8 proteins, 7 of which were shared between both conditions. Listed shared proteins are shown to the right. Bolded proteins represent proteins previously implicated in BCR signaling.

DISCUSSION

Here, we describe a new and overlooked strategy in the development of highly-selective irreversible covalent inhibitors. As a proof-of-concept, we developed fumarate-based analogues of Ibrutinib, each one possessing varying levels of steric bulk and electron-donating properties. We found that while methyl- and phenyl-fumarate ester analogues of Ibrutinib were highly reactive towards free reduced cysteine, a *t*-Bu fumarate ester possessed a reactivity comparable to that of the acrylamide-equipped parent compound. We further tested the selectivity of our analogues relative to Ibrutinib by furnishing each one with an alkyne handle and carrying out established gel- and mass spectrometry (MS)-based probe experiments. Despite having similar reactivities, the *t*-Bu fumarate ester probe was exquisitely selective for BTK in both concentration- and time-dependent labelling experiments relative to the Ibrutinib probe. This was demonstrated both qualitatively by in-gel fluorescence scanning experiments and quantitatively in SILAC-based MS experiments. Competition experiments further validated that the selectivity of the *t*-Bu fumarate ester probe analogue of Ibrutinib was also conferred by its inhibitor counterpart. Shotgun proteomics of cells treated with either Ibrutinib or the *t*-Bu fumarate ester inhibitor revealed striking differences in their relative protein abundance profiles. While treatment with Ibrutinib led to the downregulation of 107 protein relative to vehicle treated cells, treatment with the *t*-Bu fumarate ester inhibitor resulted in the downregulation of just 8 proteins. Of these 8 proteins, 7 were also downregulated by Ibrutinib treatment, and 5 out of the 7 shared downregulated proteins have been previously implicated in B-cell receptor signaling.

Our results offer yet another strategy which can be implemented in the development of more selective covalent inhibitors. Importantly, while previous methods have obtained selectivity through modifications that alter the reactivity of the electrophile, our approach achieves selectivity in a manner in which cysteine reactivity is comparable to the original inhibitor. We demonstrate that warhead structure elaboration and optimization can augment the overall inherent selectivity of covalent inhibitors in a reactivity-independent manner.

Traditionally, covalent drug discovery campaigns mainly focus on scaffold optimization. This ultimately results in unique molecules with exceptional initial selectivity towards their intended target. However, much of the off-target engagement that occurs with irreversible covalent inhibitors is time-dependent, and this undesirable reactivity may ultimately go unnoticed within the timeframe of classical screening techniques (minutes to a few hours). In addition, in the case of covalent kinase inhibitors, many inhibitors are screened exclusively for off-target kinase reactivity.24 However, our studies and others also demonstrate that many off-targets of these molecules are non-kinases.2,8,25 Creative efforts to improve the selectivity of covalent inhibitors have been reported, and in special cases where the nucleophilicity of an amino acid residue is increased due to its microenvironment, selectivity can be achieved by simply using warheads with reduced reactivity.[8] The use of warheads that form reversible covalent bonds to inhibit their targets has also been successful in developing potent and selective covalent inhibitors with a reversible MoA.26 Incorporating metabolic vulnerabilities to the warhead has led to kinetically selective covalent inhibitors which rapidly engage their intended targets but become deactivated overtime by esterases thereby minimizing any time-dependent off-target reactivity.

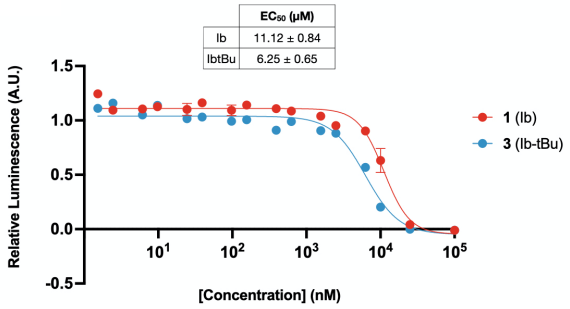

Figure 6. Determination of cytotoxicity of Ib and IbtBu inhibitors. Cell viability assay comparing the cytotoxicity profiles of Ib and IbtBu in Mino cells. Points represent the mean of three replicates and the standard error of the mean (SEM) are plotted.

Although the abovementioned methods have expanded the repertoire of electrophiles amenable to covalent inhibitors, they each have unique use-cases, thus limiting their overall utility. Therefore, more generalizable methods to increase the

selectivity of covalent probes and small molecule inhibitors are needed. We now report that elaboration of the electrophilic moiety can directly impart greater overall selectivity simply due to its own structure without a change in its reactivity or dependence on metabolic inactivation. We believe that electrophile structure optimization may be used in conjunction with scaffold optimization to obtain highly selective covalent inhibitors.

While our work represents a novel approach to improve covalent inhibitor selectivity, we recognize that it is limited to protein targets that can accept a larger electrophile, such as BTK.9 Ongoing work in our laboratory involves identifying other attractive protein targets, in particular kinases, which may also be amenable to this approach. Despite this limitation, it is worth noting that BTK has been, and continues to be, an attractive target for covalent inhibitors due to its role in the development of B-cell malignancies. Notably, as of 2020, there were 5 covalent inhibitors of BTK in clinical trials, 3 of which utilize an acrylamide warhead to carry out their inhibition.[26] Our findings presented here highlight an unprecedented optimization opportunity currently available to covalent inhibitors of BTK.

ASSOCIATED CONTENT

Supporting Information

The Supporting Information is available free of charge on the ACS Publications website.

Methods and materials (PDF)

Protein characterization (XLSX)

AUTHOR INFORMATION

Corresponding Author

Balyn W. Zaro – Department of Pharmaceutical Chemistry and Cardiovascular Research Institute University, University of California, San Francisco, CA 94305, United States; orcid

Email: Balyn.Zaro@ucsf.edu

Authors

José L. Montaño – Department of Pharmaceutical Chemistry and Cardiovascular Research Institute University, University of California, San Francisco, CA 94305, United States; orcid

Brian J. Wang – *Department of Pharmaceutical Chemistry and Cardiovascular Research Institute University, University of California, San Francisco, CA 94305, United States;* orcid

Regan F. Volk – *Department of Pharmaceutical Chemistry and Cardiovascular Research Institute University, University of California, San Francisco, CA 94305, United States;* orcid

Virginia G. Garda – *Department of Pharmaceutical Chemistry and Cardiovascular Research Institute University, University of California, San Francisco, CA 94305, United States;* orcid

Author Contributions

BWZ and JLM prepared and wrote the manuscript. Experiments were conducted by JLM, BJW, RFV and VGG. All authors have given approval of the final version of the manuscript.

Funding Sources

This work was supported through the Beckman Young Investigator Program from the Arnold O. and Mabel Beckman Foundation; a National Science Foundation Graduate Research Fellowship under grant no. DGE-2034836 (to JLM); and the University of California, San Francisco.

ACKNOWLEDGMENT

We thank M.R. Pratt for careful reading of the manuscript and S. Vigneron and L. Chen for useful discussions. JLM would also like to thank Jón Þór Birgisson *et al*. and for essential assistance.

ABBREVIATIONS

BTK, Bruton's Tyrosine Kinase; Ib, Ibrutinib; IbtBu, Ibrutinib-t-butyl; IbAlk, Ibrutinib-Alkyne; IbtBuAlk, Ibrutinib-t-butyl-alkyne.

REFERENCES

(1) Ferguson, F. M.; Gray, N. S. Kinase Inhibitors: The Road Ahead. Nature Reviews Drug Discovery 2018, 17 (5), 353–377. https://doi.org/10.1038/nrd.2018.21.

(2) Bauer, R. A. Covalent Inhibitors in Drug Discovery: From Accidental Discoveries to Avoided Liabilities and Designed Therapies. Drug Discovery Today 2015, 20 (9), 1061–1073. https://doi.org/https://doi.org/10.1016/j.drudis.2015.05.005.

(3) Lanning, B. R.; Whitby, L. R.; Dix, M. M.; Douhan, J.; Gilbert, A. M.; Hett, E. C.; Johnson, T. O.; Joslyn, C.; Kath, J. C.; Niessen, S.; Roberts, L. R.; Schnute, M. E.; Wang, C.; Hulce, J. J.; Wei, B.; Whiteley, L. O.; Hayward, M. M.; Cravatt, B. F. A Road Map to Evaluate the Proteome-Wide Selectivity of Covalent Kinase Inhibitors. Nature Chemical Biology 2014, 10 (9), 760–767. https://doi.org/10.1038/nchembio.1582.

(4) Senkane, K.; Vinogradova, E. v; Suciu, R. M.; Crowley, V. M.; Zaro, B. W.; Bradshaw, J. M.; Brameld, K. A.; Cravatt, B. F. The Proteome-Wide Potential for Reversible Covalency at Cysteine. Angewandte Chemie International Edition 2019, 58 (33), 11385–11389. https://doi.org/https://doi.org/10.1002/anie.201905829.

(5) Miller, R. M.; Paavilainen, V. O.; Krishnan, S.; Serafimova, I. M.; Taunton, J. Electrophilic Fragment-Based Design of Reversible Covalent Kinase Inhibitors. Journal of the American Chemical Society 2013, 135 (14), 5298–5301. https://doi.org/10.1021/ja401221b.

(6) Serafimova, I. M.; Pufall, M. A.; Krishnan, S.; Duda, K.; Cohen, M. S.; Maglathlin, R. L.; McFarland, J. M.; Miller, R. M.; Frödin, M.; Taunton, J. Reversible Targeting of Noncatalytic Cysteines with Chemically Tuned Electrophiles. Nature Chemical Biology 2012, 8 (5), 471–476. https://doi.org/10.1038/nchembio.925.

(7) Shindo, N.; Fuchida, H.; Sato, M.; Watari, K.; Shibata, T.; Kuwata, K.; Miura, C.; Okamoto, K.; Hatsuyama, Y.; Tokunaga, K.; Sakamoto, S.; Morimoto, S.; Abe, Y.; Shiroishi, M.; Caaveiro, J. M. M.; Ueda, T.; Tamura, T.; Matsunaga, N.; Nakao, T.; Koyanagi, S.; Ohdo, S.; Yamaguchi, Y.; Hamachi, I.; Ono, M.; Ojida, A. Selective and Reversible Modification of Kinase Cysteines with Chlorofluoroacetamides. Nature Chemical Biology 2019, 15 (3), 250–258. https://doi.org/10.1038/s41589-018-0204-3.

(8) Barf, T.; Covey, T.; Izumi, R.; van de Kar, B.; Gulrajani, M.; van Lith, B.; van Hoek, M.; de Zwart, E.; Mittag, D.; Demont, D.; Verkaik, S.; Krantz, F.; Pearson, P. G.; Ulrich, R.; Kaptein, A. Acalabrutinib (ACP-196): A Covalent Bruton Tyrosine Kinase Inhibitor with a Differentiated Selectivity and In Vivo Potency Profile. Journal of Pharmacology and Experimental Therapeutics 2017, 363 (2), 240 LP – 252. https://doi.org/10.1124/jpet.117.242909.

(9) Reddi, R. N.; Resnick, E.; Rogel, A.; Rao, B. V.; Gabizon, R.; Goldenberg, K.; Gurwicz, N.; Zaidman, D.; Plotnikov, A.; Barr, H.; Shulman, Z.; London, N. Tunable Methacrylamides for Covalent Ligand Directed Release Chemistry. Journal of the American Chemical Society 2021, 143 (13), 4979–4992. https://doi.org/10.1021/jacs.0c10644.

(10) Zaro, B. W.; Whitby, L. R.; Lum, K. M.; Cravatt, B. F. Metabolically Labile Fumarate Esters Impart Kinetic Selectivity to Irreversible Inhibitors. Journal of the American Chemical Society 2016, 138 (49), 15841–15844. https://doi.org/10.1021/jacs.6b10589.

(11) Bender, A. T.; Gardberg, A.; Pereira, A.; Johnson, T.; Wu, Y.; Grenningloh, R.; Head, J.; Morandi, F.; Haselmayer, P.; Liu-Bujalski, L. Ability of Bruton's Tyrosine Kinase Inhibitors to Sequester Y551 and Prevent Phosphorylation Determines Potency for Inhibition of Fc Receptor but Not B-Cell Receptor Signaling. Molecular Pharmacology 2017, 91 (3), 208 LP – 219. https://doi.org/10.1124/mol.116.107037.

(12) Speers, A. E.; Adam, G. C.; Cravatt, B. F. Activity-Based Protein Profiling in Vivo Using a Copper(I)-Catalyzed Azide-Alkyne [3 + 2] Cycloaddition. Journal of the American Chemical Society 2003, 125 (16), 4686–4687. https://doi.org/10.1021/ja034490h.

(13) Parker, C. G.; Pratt, M. R. Click Chemistry in Proteomic Investigations. Cell 2020, 180 (4), 605–632. https://doi.org/https://doi.org/10.1016/j.cell.2020.01.025.

(14) Liu, Q.; Sabnis, Y.; Zhao, Z.; Zhang, T.; Buhrlage, S. J.; Jones, L. H.; Gray, N. S. Developing Irreversible Inhibitors of the Protein Kinase Cysteinome. Chemistry & Biology 2013, 20 (2), 146–159. https://doi.org/https://doi.org/10.1016/j.chembiol.2012.12.006.

(15) Hondares, E.; Brown, M. A.; Musset, B.; Morgan, D.; Cherny, V. v; Taubert, C.; Bhamrah, M. K.; Coe, D.; Marelli-Berg, F.; Gribben, J. G.; Dyer, M. J. S.; DeCoursey, T. E.; Capasso, M. Enhanced Activation of an Amino-Terminally Truncated Isoform of the Voltage-Gated Proton Channel HVCN1 Enriched in Malignant B Cells. Proceedings of the National Academy of Sciences 2014, 111 (50), 18078 LP – 18083. https://doi.org/10.1073/pnas.1411390111.

(16) Capasso, M.; Bhamrah, M. K.; Henley, T.; Boyd, R. S.; Langlais, C.; Cain, K.; Dinsdale, D.; Pulford, K.; Khan, M.; Musset, B.; Cherny, V. v; Morgan, D.; Gascoyne, R. D.; Vigorito, E.; DeCoursey, T. E.; MacLennan, I. C. M.; Dyer, M. J. S. HVCN1 Modulates BCR Signal Strength via Regulation of BCR-Dependent Generation of Reactive Oxygen Species. Nature Immunology 2010, 11 (3), 265–272. https://doi.org/10.1038/ni.1843.

(17) Nagel, D.; Vincendeau, M.; Eitelhuber, A. C.; Krappmann, D. Mechanisms and Consequences of Constitutive NF-KB Activation in B-Cell Lymphoid Malignancies. Oncogene 2014, 33 (50), 5655–5665. https://doi.org/10.1038/onc.2013.565.

(18) de Silva, N. S.; Anderson, M. M.; Carette, A.; Silva, K.; Heise, N.; Bhagat, G.; Klein, U. Transcription Factors of the Alternative NF-KB Pathway Are Required for Germinal Center B-Cell Development. Proceedings of the National Academy of Sciences 2016, 113 (32), 9063 LP – 9068. https://doi.org/10.1073/pnas.1602728113.

(19) Holland, J.; Owens, T. Signaling through Intercellular Adhesion Molecule 1 (ICAM-1) in a B Cell Lymphoma Line: THE ACTIVATION OF Lyn TYROSINE KINASE AND THE MITOGEN-ACTIVATED PROTEIN KINASE PATHWAY *. Journal of Biological Chemistry 1997, 272 (14), 9108–9112. https://doi.org/10.1074/jbc.272.14.9108.

(20) Dennig, D.; Lacerda, J.; Yan, Y.; Gasparetto, C.; O'Reilly, R. J. ICAM-1 (CD54) Expression on B Lymphocytes Is Associated with Their Costimulatory Function and Can Be Increased by Coactivation with IL-1 and IL-7. Cellular Immunology 1994, 156 (2), 414–423. https://doi.org/https://doi.org/10.1006/cimm.1994.1186.

(21) Sana, I.; Mantione, M. E.; Angelillo, P.; Muzio, M. Role of NFAT in Chronic Lymphocytic Leukemia and Other B-Cell Malignancies . Frontiers in Oncology . 2021, p 1044.

(22) Giampaolo, S.; Wójcik, G.; Klein-Hessling, S.; Serfling, E.; Patra, A. K. B Cell Development Is Critically Dependent on NFATc1 Activity. Cellular & Molecular Immunology 2019, 16 (5), 508–520. https://doi.org/10.1038/s41423-018-0052-9.

(23) Uitdehaag, J. C. M.; Verkaar, F.; Alwan, H.; de Man, J.; Buijsman, R. C.; Zaman, G. J. R. A Guide to Picking the Most Selective Kinase Inhibitor Tool Compounds for Pharmacological Validation of Drug Targets. British journal of pharmacology 2012, 166 (3), 858–876. https://doi.org/10.1111/j.1476-5381.2012.01859.x.

(24) Susan, K.; Stephanie, H.; Mathias, W.; Harald, P.; Binje, V.; Paul-Albert, K.; Maria, R.; Benjamin, R.; Svenja, P.; Chen, M.; Jana, Z.; Katrin, R.; Huichao, Q.; Dominic, H.; Heiner, K.; Melanie, S.; Giulia, C.; Elena, C.; Re, D. S.; Annette, F.; Zhixiang, W.; Tobias, S.; Lars, R.; Wilhelm, B.; Jan, H.; Anne-Kathrin, G.; Bjoern-Oliver, G.; Paul, Z. D.; Gian, K.; Tonu, V.; Robert, P.; Hannes, H.; Neeme, T.; Karl, K.; Katharina, G.; Florian, B.; Judith, S.; Hans-Christian, E.; Stephan, A.; Axel, W.; A., G. P.; Sabine, S.; Rudolf, F. E.; Juergen, R.; Guillaume, M.; Irmela, J.; Karsten, S.; Bernhard, K. The Target Landscape of Clinical Kinase Drugs. Science 2017, 358 (6367), eaan4368. https://doi.org/10.1126/science.aan4368.

(25) Bradshaw, J. M.; McFarland, J. M.; Paavilainen, V. O.; Bisconte, A.; Tam, D.; Phan, V. T.; Romanov, S.; Finkle, D.; Shu, J.; Patel, V.; Ton, T.; Li, X.; Loughhead, D. G.; Nunn, P. A.; Karr, D. E.; Gerritsen, M. E.; Funk, J. O.; Owens, T. D.; Verner, E.; Brameld, K. A.; Hill, R. J.; Goldstein, D. M.; Taunton, J. Prolonged and Tunable Residence Time Using Reversible Covalent Kinase Inhibitors. Nature Chemical Biology 2015, 11 (7), 525–531. https://doi.org/10.1038/nchembio.1817.

(26) Sutanto, F.; Konstantinidou, M.; Dömling, A. Covalent Inhibitors: A Rational Approach to Drug Discovery. RSC Medicinal Chemistry 2020, 11 (8), 876–884. https://doi.org/10.1039/D0MD00154F.

SUPPORTING INFORMATION

Improved Electrophile Design for Exquisite Covalent Molecule Selectivity

José L. Montaño, Brian J. Wang, Regan F. Volk, Virginia G. Garda, Balyn W. Zaro*

Department of Pharmaceutical Chemistry and Cardiovascular Research Institute, University of California, San Francisco, California 94158, United States.

* Correspondence to: Balyn W. Zaro, balyn.zaro@ucsf.edu

Table of Contents

I. Supplementary Figures

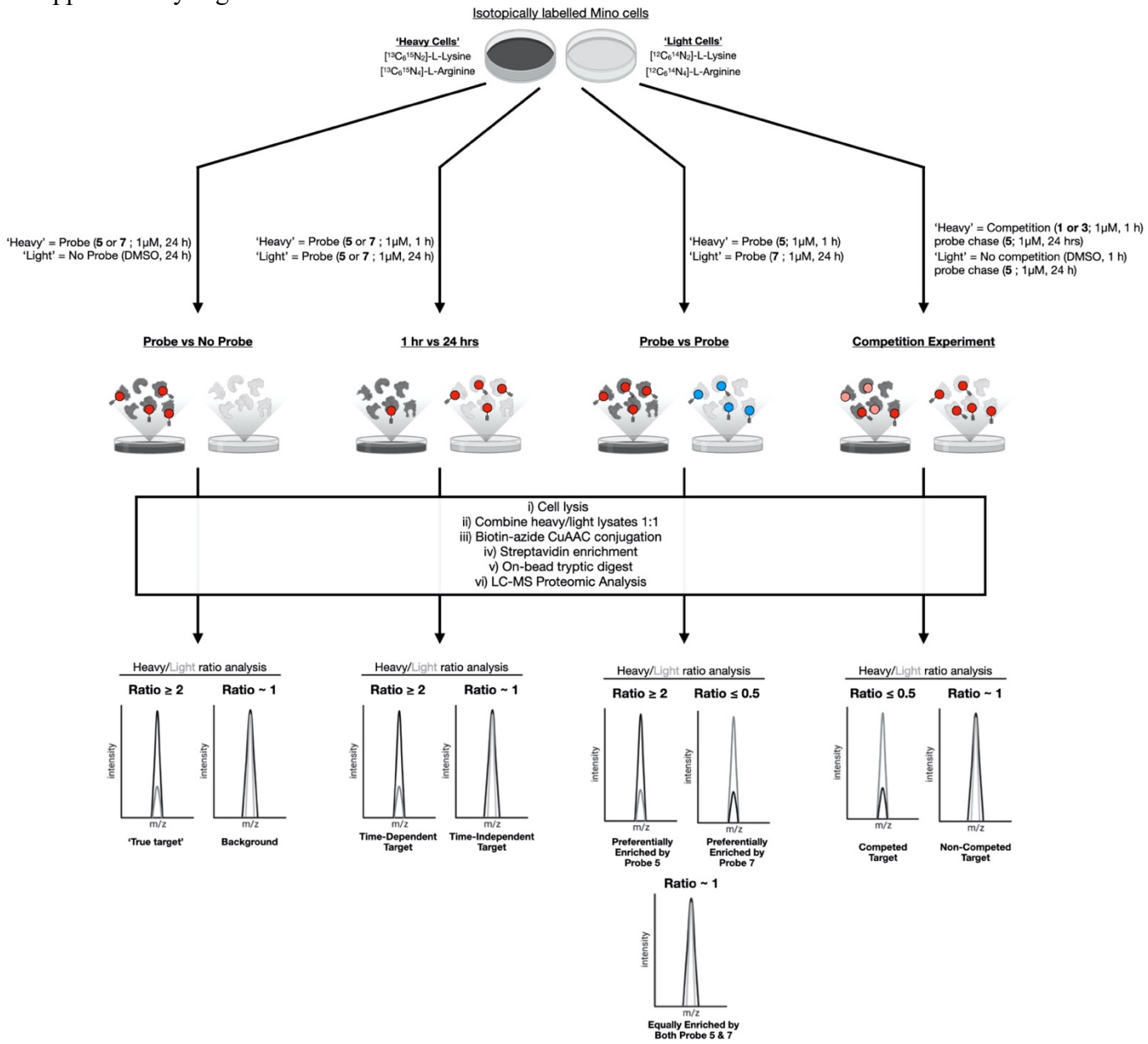

Figure S1. General workflow of all SILAC experiments conducted in this study. In each case, isotopically labelled 'heavy' and 'light' Mino cells were treated with the indicated conditions. After treatment, heavy and light cells were lysed and their proteins quantified. Heavy and light proteomes were mixed 1:1 prior to biotin-azide conjugation via click chemistry. Biotin-tagged proteins were enriched for using streptavidin-coated resin followed by on-bead tryptic digest. Finally, peptide samples were prepared for LC-MS analysis. Examples of heavy/light ratio analysis and the cut-off's applied in each experiment are indicated below.

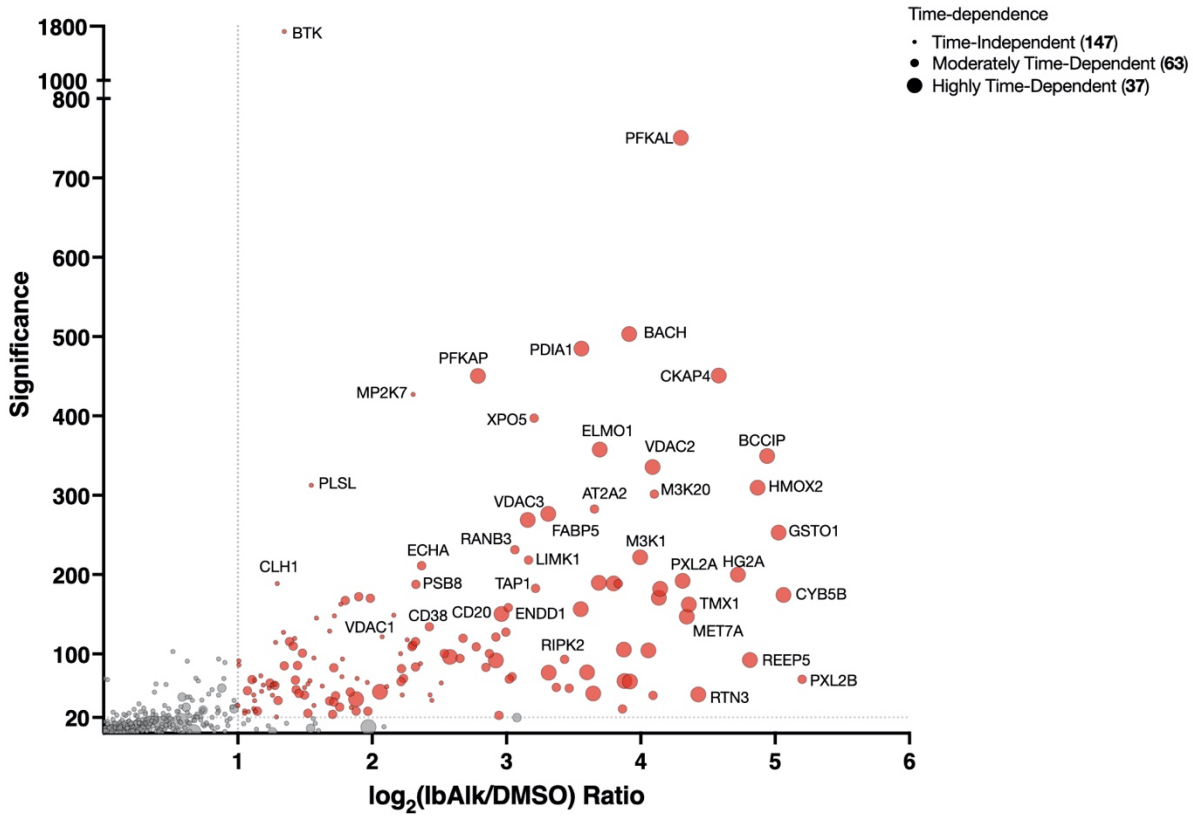

Figure S2. Proteins significantly enriched by IbAlk as determined from probe vs no probe experiments.

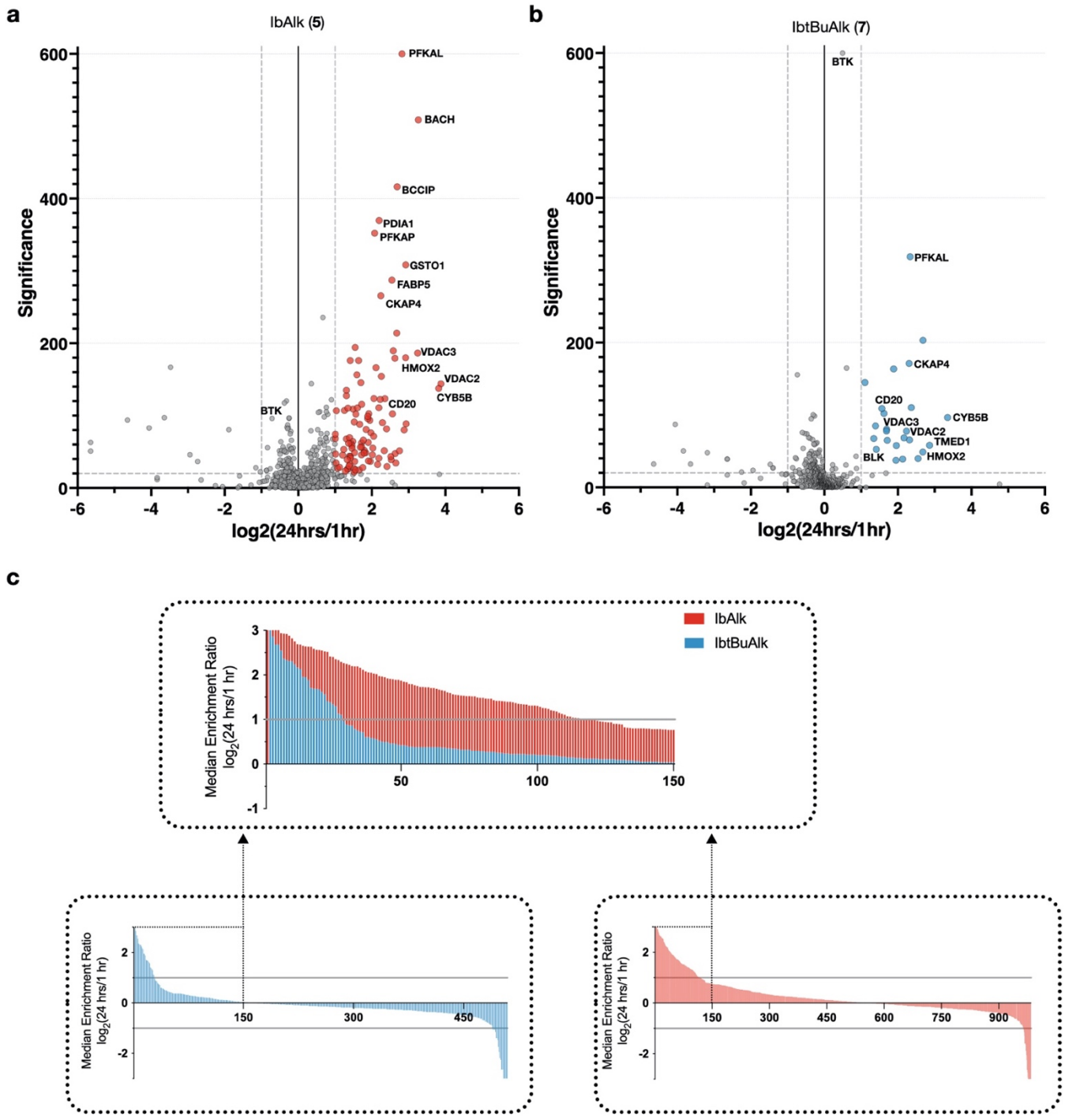

Figure S3. Determination of time-dependent targets of IbAlk and IbtBuAlk. (a) Volcano plot of proteins enriched in a time-dependent manner by IbAlk and (b) IbtBuAlk. Enriched proteins with 24h/1h ratios of ≥ 2 and significance values of ≥ 20 were categorized as time-dependent targets. (c) Comparison of the overall number of time-dependent targets between IbAlk and IbtBuAlk. In order of descending SILAC ratio, the top 150 proteins for each probe were taken and overlaid. While IbAlk has 100 time-dependent targets, IbtBuAlk has only 28.

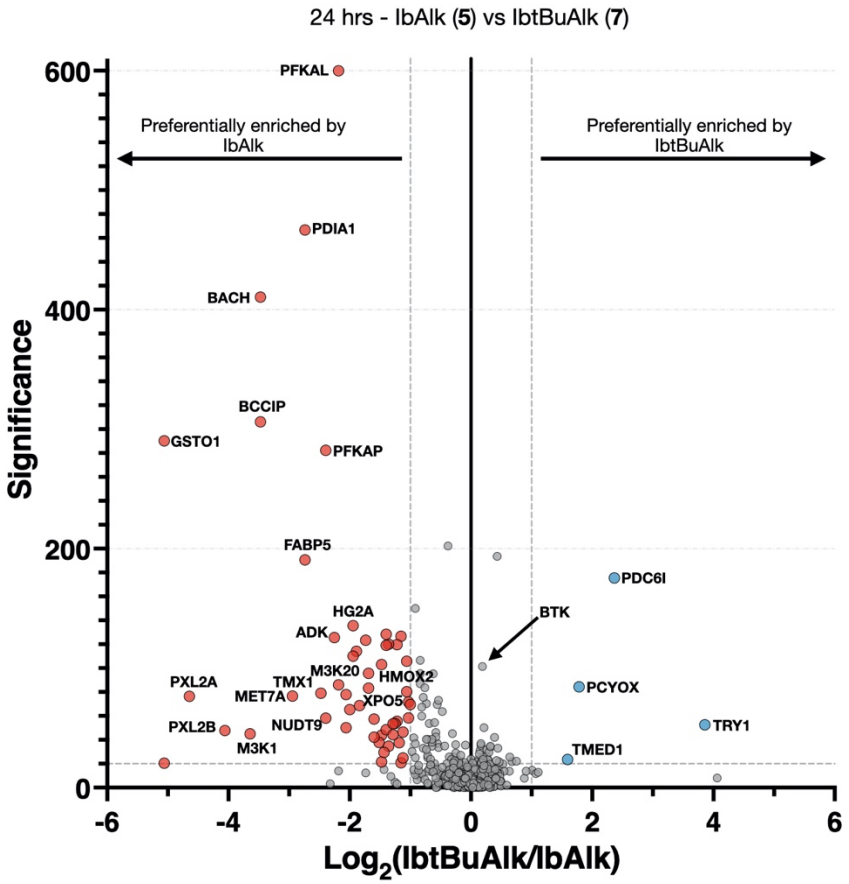

Figure S4. Proteins preferentially enriched by IbAlk or IbtBuAlk as determined by probe vs probe SILAC experiments. Heavy and light isotopically labelled Mino cells were treated with 5 (1 uM, 24 hrs) or 7 (1 uM, 24 hrs), respectively. Proteins were considered as preferentially enriched by IbAlk were required to have (IbtBuAlk/IbAlk) SILAC ratios ≤ 0.5 and significance values ≥ 20, whereas proteins preferentially enriched by IbtBuAlk were required to have SILAC ratios ≥ 2.

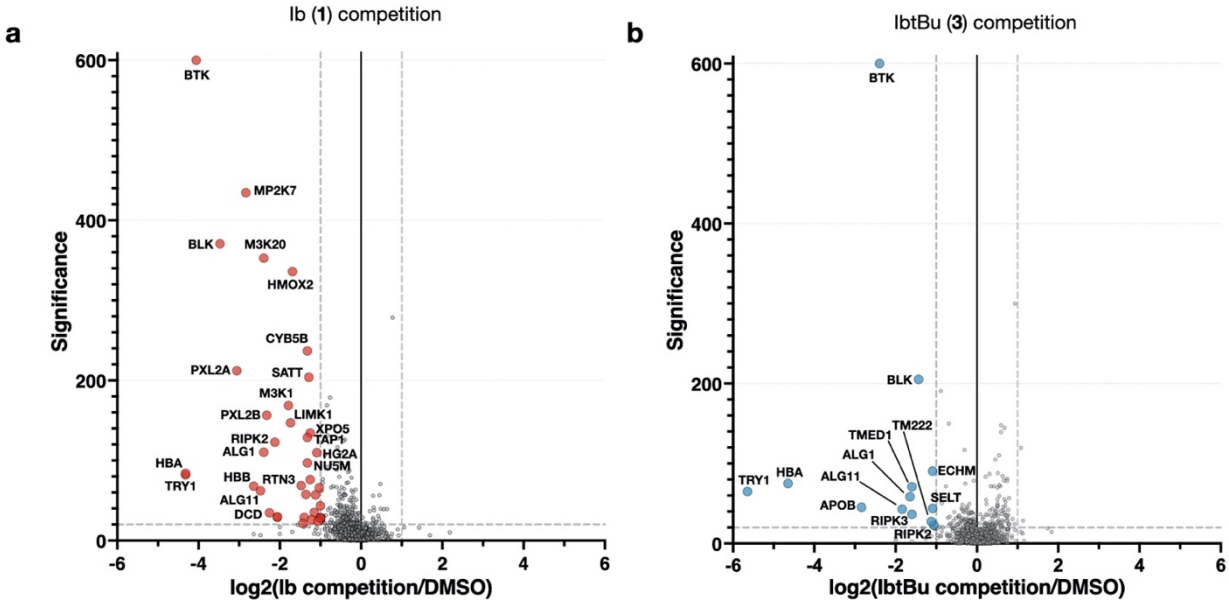

Figure S5. Characterization of proteins competed away by Ib and IbtBu inhibitors. (a and b) Heavy and light SILAC Mino cells were pre-treated with either inhibitor (1 or 3; 1 uM, 1 h) or DMSO (1 h), respectively. After pre-treatments, both heavy and light cells were chased with probe (5; 1 uM, 24 h). Proteins with (competition/DMSO) SILAC ratios ≤ 0.5 and significance values ≥ 20 were considered to be competed targets.

II. Biological Methods

Cell Culture.
Mino cells were cultured in RPMI media with L-glutamine (Gibco) and supplemented with 15% fetal bovine serum (HyClone) and Penicillin/Streptomycin (100 µg/mL). All cell lines were maintained in a humidified incubator at 37 °C and 5.0% CO_2.

***In situ* cell labeling – time course ABPP experiments.**
Mino cell cultures (1×10^6 cells/condition) were treated with indicated probe (1 µM) in RPMI media containing 15% FBS and penicillin/streptomycin for 1 – 24 h at 37 °C. Upon treatment completion, cells were harvested and transferred to conical tubes. Cells were pelleted (1,000 x g, 4 min, 4 °C), washed with ice-cold DPBS and pelleted again (2x, 1,000 x g, 4 min, 4 °C). Washed pellets were resuspended in ice-cold DPBS and sonicated (2 x 10 pulses, 20% amplitude, 1 s pulse rate). The lysed suspension was pelleted (21,000 x g, 25 min, 4 °C) and the supernatant was transferred to a conical tube. Protein concentrations were determined by BCA assay (Thermo Scientific) and further diluted to 0.5 - 1 mg/mL prior to CuAAC.

***In situ* cell labeling – concentration course ABPP experiments**
Mino cells were treated with indicated probe (1 nM – 1 µM) in RPMI media containing 15% FBS and penicillin/streptomycin for 16 h at 37 °C. Cells were harvested and prepared for CuAAC as described above.

***In situ* cell labeling – competition ABPP experiments.**
Mino cells were treated with indicated inhibitor (10 µM) in RPMI media containing 15% FBS and penicillin/streptomycin for 1 h at 37 °C. Treatments were then chased with indicated probe (1 µM) for 16 h at 37 °C. Upon treatment completion, cells were harvested and prepared for CuAAC as described above.

Cu(I)-Catalyzed [3 + 2] Azide-Alkyne Cycloaddition (CuAAC).
For in-gel fluorescence scanning experiments, a click chemistry cocktail was prepared fresh [TAMRA-azide (25 µM, 1.25 mM stock solution in DMSO); tris(2-carboxyethyl)phosphine hydrochloride (TCEP) (1 mM, 50 mM freshly prepared stock solution in water); tris[(1-benzyl-1-H-1,2,3-triazol-4-yl)methyl]amine (TBTA) (100 µM, 1.7 mM stock solution 3:1 *tert*-butanol:DMSO); $CuSO_4 \bullet 5H_2O$ (1 mM, 50 mM stock solution in water)]. Click chemistry cocktail (6 uL) was then added to each cell lysate sample (50 uL; 0.5-1 ug/uL protein concentration) for a total reaction volume of 56 µL. The reaction was gently vortexed and reacted at room temperature for 1 hour. The reaction was quenched by the addition of ice-cold methanol (250 µL), and the mixture was stored at -20 °C for 2 h or overnight. The precipitated protein were pelleted (10,000 x g, 10 min, 4 °C) and the supernatant was discarded. Tubes were left to dry inverted for 30 min to ensure that methanol had completely evaporated. The protein pellets were resuspended with 4% SDS in PBS (pH 7.5) (22.5 µL) and bath sonicated into solution (35 kHz, 10 min). Upon completion, 7.5 µL of 4x loading buffer (Bio-rad Laemmli Sample Buffer, 10% ß-mercaptoethanol) was added. The mixture was gently vortexed and boiled at 95 °C for 5 min. After cooling to room temperature, 20 µg of protein was loaded per lane for SDS-PAGE separation on a 4-15% Tris-Glycine gel (Bio-Rad, Criterion TGX).

In-gel Fluorescence Scanning.
Following SDS-PAGE separation, gels were scanned on a ChemiDoc MP (Bio-Rad) using the green epi illumination excitation light source and a 602/50 filter.

ABPP-SILAC Sample preparation.
All SILAC experiments were conducted using isotopically labelled Mino cells (generated by 6 passages in light (100 µg/mL L-arginine and L-lysine) or heavy (100 µg/mL $^{13}C_6{}^{15}N_4$ L-arginine and $^{13}C_6{}^{15}N_2$ L-lysine, Cambridge Isotope Laboratories) media (SILAC RPMI 1640 (ThermoScientific), supplemented with 15% dialyzed FBS and penicillin/streptomycin). The conditions for each SILAC experiment conducted in this study are as follows:

SILAC Experiment	**Heavy Mino cells** (3 mL, 10^6 cells/mL)	**Light Mino cells** (3 mL, 10^6 cells/mL)
Probe vs no probe	**5** or **7** (1 μM, 24 h)	DMSO (24 h)
1 hour vs 24 hours	**5** or **7** (1 μM, 24 h)	**5** or **7** (1 μM, 1 h)
Probe vs Probe	**5** (1 μM, 24 h)	**7** (1 μM, 24 h)
Competition	**1** or **3** (10 μM, 1 h) followed by **5** (1 μM, 24 h)	DMSO (1 h) followed by **5** (1 μM, 24 h)

Upon treatment completion, cells were transferred to conical tubes, pelleted (1,000 x g, 4 min, 4 ℃), washed with ice-cold DPBS (2x 1,000 x g, 4 min, 4 ℃) and pelleted again. Washed pellets were resuspended in ice-cold PBS and sonicated (2 x 10 pulses, 20% amplitude, 1 s pulse rate). Lysed samples were pelleted (21,000 x g, 10 min, 4 ℃) and supernatants were transferred to conical tubes. The protein concentration was determined by BCA Assay (ThermoScientific) and each heavy and light pair was then combined 1:1 (250 μg protein of each) and brought to a final volume of 500 μL with DPBS. Each CuAAC reagent was added stepwise to the sample [biotin-azide (5 μL, 100 μM final concentration, 5 mM stock solution in DMSO); tris(2-carboxyethyl)phosphine hydrochloride (TCEP) (10 μL, final concentration 1 mM, 50 mM freshly prepared stock solution in water); tris[(1-benzyl-1-H-1,2,3-triazol-4-yl)methyl]amine (TBTA) (30 μL, final concentration 100 μM, 1.7 mM stock solution in 3:1 *tert*-butanol:DMSO); $CuSO_4$•$5H_2O$ (10 μL, final concentration 1 mM, 50 mM freshly prepared stock solution in water). The reaction was gently vortexed and incubated at rt on a rotator for 1 h.

Following reaction completion, the reaction was quenched with 1 mL ice-cold methanol and vortexed. Ice-cold chloroform (250 μL) and ice-cold water (500 μL) was then added, and the mixture was vortexed into a milky solution. Samples were then centrifuged to generate a protein disc at the organic/aqueous interface (4,300 x g, 10 min, 4 ℃). The organic layer was removed from the bottom, leaving the disc to stick to the side of the tube and allowing the aqueous to be decanted. The pellet was washed 2x with 1:1 methanol:chloroform and sonicated back into ice-cold methanol (1 mL). Ice-cold chloroform was added to each sample (250 μL) and centrifuged (5,000 x g, 10 min). Supernatants were discarded and protein pellets were allowed to dry for a few minutes until most of the solvent was gone.

Freshly prepared urea (6 M in PBS, 500 μL) was added to each dried protein pellet. A solution of freshly prepared 1:1 TCEP (200 mM in water stock) and K_2CO_3 (600 mM in water stock) was added to each sample (50 μL) followed by addition of 10% SDS in PBS (10 μL). The protein pellet was resuspended by sonication and the resulting mixture was incubated with shaking (37 ℃, 30 min). Following incubation, iodoacetamide (70 μL, 400 mM in PBS stock) was added, and the mixture was incubated in the dark for 30 min at rt. Upon completion of alkylation the reaction was quenched with 10% SDS in PBS (130 μL). The sample was further diluted with PBS (6 mL). The diluted proteome was mixed and sonicated briefly.

Avidin beads (pre-washed 2x with 10 mL PBS) were added to each sample, and the samples were incubated at rt on a rotator for 2 h. The beads were pelleted (1600 x g, 2 min) and supernatant removed by aspiration. Beads were washed with 0.2% SDS in PBS (1x, 5 mL), PBS (2x, 5 mL), and water (1x, 5 mL) with pelleting after each wash (2600 x g, 2 min). Beads were transferred to a protein Lo-Bind eppi tube (Eppendorf) in water (2x, 500 μL) and resuspended in freshly prepared 2 M Urea in 25 mM ammonium bicarbonate (100 μL). Trypsin (1 μg) was then added to each sample and samples were digested with shaking (16 – 18 h, 37 ℃).

Following digestion, samples were transferred to a Bio-Spin column (Bio-Rad) and spun (800 x g, 30 s). The beads were further washed with PBS (100 μL) and spun (800 x g, 30 s). The sample was stored at -20 ℃ until LC-MS/MS analysis.

Sample Preparation of Inhibitor Treated Mino Cells for MS Analysis

In duplicate, Mino cells (10^6 cells) in media (3 mL) were dosed with 3 μL of either inhibitor (**1** or **3**, 1 mM) or DMSO for 48 hours. Upon treatment completion, cells were harvested, lysed and prepared for bottom-up MS

analysis using the iST PreOmics kit as per the manufacturer's instructions. Samples were analyzed as described below.

Mass spectrometry data acquistion and analysis.

Mass spectrometry analysis – liquid chromatography and timsTOF Pro

A nanoElute was attached in line to a timsTOF Pro equipped with a CaptiveSpray Source (Bruker, Hamburg, Germany). Chromatography was conducted at 40°C through a 25cm reversed-phase C18 column (PepSep) at a constant flow-rate of 0.5 µL/min. Mobile phase A was 98/2/0.1% Water/MeCN/Formic Acid (v/v/v) and phase B was MeCN with 0.1% Formic Acid (v/v). During a 108 min method, peptides were separated by a 3-step linear gradient (5% to 30% B over 90 min, 30% to 35% B over 10 min, 35% to 95% B over 4 min) followed by a 4 min isocratic flush at 95% for 4 min before washing and a return to low organic conditions. Experiments were run as data-dependent acquisitions with ion mobility activated in PASEF mode. MS and MS/MS spectra were collected with m/z 100 to 1700 and ions with $z = +1$ were excluded.

Raw data files were searched using PEAKS Online Xpro 1.6 (Bioinformatics Solutions Inc., Waterloo, Ontario, Canada). The precursor mass error tolerance and fragment mass error tolerance were set to 20 PPM and 0.03 respectively. The trypsin digest mode was set to semi-specific and missed cleavages was set to 2. The human Swiss-Prot reviewed (canonical) database (downloaded from UniProt) and the common repository of adventitious proteins (cRAP, downloaded from The Global Proteome Machine Organization) totaling 20,487 entries were used. Carbamidomethylation was selected as a fixed modification. Deamidation (NQ), Oxidation (M), 13C(6) 15N(2) Silac label, and 13C(6) 15N(4) Silac label, were selected as variable modifications.

All ABPP-SILAC experiments were repeated in at least triplicate and combined datasets subjected to the following filtration criteria:

1. During the PEAKS Online Xpro export process, a false discovery rate (FDR) cutoff for peptide identification was applied and only peptides with FDR ≤ 1% were included.
2. For probe vs no probe experiments, proteins were required to have been quantified in at least one out of the four separate biological replicates in order to identify all potential putative targets of each probe. For all other SILAC experiments, proteins were required to have been quantified in two out of three biological replicates.
3. Proteins either flagged by the cRAP database or containing 'Keratin,' 'Statherin,' 'Serum albumin,' 'Hornerin,' 'Trypsin' were dropped.
4. Proteins had to contain ≥ 2 unique quantified filtered peptides (# unique) and ≥ 3 quantified peptides (# peptides).
5. Proteins were required to have Significance values ≥ 20.
6. The median enrichment ratio of proteins was required to be ≥ 2.0-fold.

For assessing global proteomic changes as a result of inhibitor treatment, duplicate samples were prepared for each condition, and each sample was injected twice for MS analysis. The average total area for each protein identified in each condition was used to generate relative abundance ratios. Proteins were considered as downregulated or upregulated if their inhibitor/DMSO area ratios were ≤ 0.5 or ≥ 2, respectively.

Cytotoxicity

Cell viability was determined by measuring ATP levels using CellTiter-Glo (Promega) according to the manufacturer's instructions. Briefly, 80 uL of Mino cells at 62,500 cell/mL in media (5,000 cells/well) were plated onto a 96-well assay plate (Corning). Inhibitors **1** and **3** were prepared as 5x stocks in media containing 2.5% DMSO and 20 uL of each stock was added to each well in triplicate. Assay plate was incubated at 37 °C and 5.0% CO_2 for 48 hours prior to the addition of prepared CellTiter-Glo reagent. Assay plate was incubated at RT for 20 min with gentle rocking. Finally, luminescence was read (0.5 sec integration time) on a plate reader (Cytation 5, BioTek).

Cysteine Reactivity Assay

L-cysteine was prepared at a concentration of 250 μM in assay buffer (100 mM Tris pH 9.0, 50% MeOH as co-solvent). In triplicate, 100 μL of L-cysteine (250 μM) in assay buffer was added to each well in a clear, flat-bottom 96-well plate (Greiner Bio-one). To each well was then added 1 μL of 100x inhibitor stocks in DMSO (final concentration 500 μM) or DMSO vehicle and incubated at room temperature for the indicated time (0-60 min). Upon incubation completion, Ellman's reagent (Thermo) (10 μL, 50 mM stock in DMSO, final concentration 5 mM) was added and the reaction incubated at room temperature for 10 minutes. The absorbance was measured at 412 nm on a plate reader (Cytation 5, BioTek). The remaining concentration of free cysteines was determined by a concentration curve. Second-order rate constants were determined according to previous reports.

III. Synthetic Methods and Compound Characterization

Inhibitor **2**, Probe **5** and Probe **6** were synthesized according to literature procedure. Probe **5** is available through Sigma Aldrich (Item #PZ0242). Inhibitor **1** (Ibrutinib) is widely available through several vendors.

Compounds **9** (inhibitor precursor) and **10** (probe precursor) were synthesized according to literature procedure (Lanning et. al.).

Compound **3** (Ibrutinib-t-Butyl)

tert-butyl (2E)-4-[(3R)-3-[4-amino-3-(4-phenoxyphenyl)pyrazolo[3,4-d]pyrimidin-1-yl]piperidin-1-yl]-4-oxobut-2-enoate

To a stirred mixture of 3-(4-phenoxyphenyl)-1-[(3R)-piperidin-3-yl]pyrazolo[3,4-d]pyrimidin-4-amine (**9,** 600 mg, 1.55 mmol, 1.00 equiv) and (2E)-4-(tert-butoxy)-4-oxobut-2-enoic acid (401 mg, 2.32 mmol, 1.50 equiv) in DMF (10 mL) were added DIEA (602 mg, 4.65 mmol, 3.00 equiv) and T3P (741 mg, 2.32 mmol, 1.50 equiv, 50%). The resulting mixture was stirred for 1 h at 25 °C. The mixture was poured into ice/water (400 mL) and extracted with EtOAc (3 x 400 mL). The combined organic layers were washed with brine (800 L), dried over anhydrous sodium sulfate and concentrated under reduced pressure. The residue was purified by silica gel column chromatography, eluted with CH_2Cl_2 / MeOH (5:1). The crude product was purified by Prep-HPLC with the following conditions: Column, XBridge Shield RP18 OBD Column, 5um,19x150mm; mobile phase, water (10 mM NH_4HCO_3 0.1%$NH_3.H_2O$) and ACN (35.0% ACN up to 65.0% in 7 min); Detector, 254nm. The collected fraction was lyophilized to afford tert-butyl (2E)-4-[(3R)-3-[4-amino-3-(4-phenoxyphenyl)pyrazolo[3,4-d]pyrimidin-1-yl]piperidin-1-yl]-4-oxobut-2-enoate (**3,** 114.4mg,14%) as an off-white solid. ^{1}H NMR (400 MHz, Methanol-d_4) δ 8.24 (s, 1H), 7.66 (d, *J* = 10.8 Hz, 2H), 7.45-7.37 (m, 3H), 7.20-7.07 (m, 5H), 6.56-6.29 (m, 1H), 4.93-4.90 (m, 1H), 4.55-3.38 (m, 4H), 2.50-2.05 (m, 3H), 1.81-1.65 (m, 1H), 1.50-1.42 (m, 9H). LCMS (ES, m/z): 541.25 $[M+H]^+$.

Compound **4** (Ibrutinib-phenyl)

phenyl (2E)-4-[(3R)-3-[4-amino-3-(4-phenoxyphenyl)pyrazolo[3,4-d]pyrimidin-1-yl]piperidin-1-yl]-4-oxobut-2-enoate

To a stirred mixture of 3-(4-phenoxyphenyl)-1-[(3R)-piperidin-3-yl]pyrazolo[3,4-d]pyrimidin-4-amine (**9,** 600 mg, 1.55 mmol, 1.00 equiv) and (2E)-4-oxo-4-phenoxybut-2-enoic acid (298 mg, 1.55 mmol, 1.00 equiv) in DMF (8 mL) were added DIEA (602 mg, 4.65 mmol, 3.00 equiv) and T3P (1.48 g, 2.33 mmol, 1.50 equiv, 50%). The resulting mixture was stirred for 1 h at 25 °C. The mixture was poured into ice/water (400 mL) and extracted with EtOAc (3 x 400 mL). The combined organic layers were washed with brine (800 L), dried over anhydrous sodium sulfate and concentrated under reduced pressure. The residue was purified by silica gel column chromatography, eluted with CH2Cl2 / MeOH (5:1). The crude product was purified by Prep-HPLC with the following conditions: Column, XBridge Shield RP18 OBD Column, 5um,19x150mm; mobile phase, water (10 mM NH_4HCO_3 0.1%$NH_3.H_2O$) and ACN (35.0% ACN up to 65.0% in 7 min); Detector, 254nm. The collected fraction was lyophilized to afford phenyl (2E)-4-[(3R)-3-[4-amino-3-(4-phenoxyphenyl)pyrazolo[3,4-d]pyrimidin-1-yl]piperidin-1-yl]-4-oxobut-2-enoate (**4**, 150.7 mg, 17%) as an off-white solid. ^{1}H NMR (300 MHz, Methanol-d_4) δ 8.25-8.23 (m, 1H), 7.74-7.65 (m, 2H), 7.52-7.29 (m, 5H), 7.27-7.00 (m, 8H), 6.84-6.56 (m, 1H), 4.94-4.91 (m, 1H), 4.55-3.40 (m, 4H), 2.50-2.10 (m, 3H), 1.84-1.60 (m, 1H). LCMS (ES, m/z): 561.20 $[M+H]^+$.

Compound **7** (Ibrutinib-t-Butyl-alkyne)

tert-butyl (2E)-4-[(3R)-3-[4-amino-3-[4-(3-ethynylphenoxy)phenyl]pyrazolo[3,4-d]pyrimidin-1-yl]piperidin-1-yl]-4-oxobut-2-enoate

To a stirred mixture of 3-[4-(3-ethynylphenoxy)phenyl]-1-[(3R)-piperidin-3-yl]pyrazolo[3,4-d]pyrimidin-4-amine (320 mg, 0.78 mmol, 1.00 equiv) and (2E)-4-(tert-butoxy)-4-oxobut-2-enoic acid (174 mg, 1.01 mmol, 1.3 equiv) in DMF (5 mL) were added T3P (744 mg, 1.16 mmol, 1.5 equiv, 50%) and DIEA (302 mg, 2.33 mmol, 3 equiv). The resulting mixture was stirred for 1 h at 25 ℃. The resulting mixture was poured into water (150 mL) and extracted with CH2Cl2 (3 x 150 mL). The combined organic layers were washed with brine (2 x 150 mL), dried over anhydrous Na2SO4, filtered and concentrated under reduced pressure, Then the residue was purified by silica gel column chromatography, eluted with CH2Cl2 / MeOH (10:1). The crude product was purified by Prep-HPLC with the following conditions: Column, XBridge Shield RP18 OBD Column, 19x250 mm, 10um; mobile phase, water (10 mmol/L NH4HCO3+0.1%NH3.H2O) and ACN (53% PhaseB up to 68% in 10 min); Detector, UV 254 nm. The collected fraction was lyophilized to afford tert-butyl (2E)-4-[(3R)-3-[4-amino-3-[4-(3-ethynylphenoxy)phenyl]pyrazolo[3,4-d]pyrimidin-1-yl]piperidin-1-yl]-4-oxobut-2-enoate (53.1 mg, 13.12%) as a white solid. ^{1}H-NMR-PH-UKS-2020-018-9-0 (400 MHz, CD3OD) δ (ppm): 8.25 (s, 1H), 7.71-7.68 (m, 2H), 7.45-7.10 (m, 7H), 6.56-6.28 (m, 1H), 4.93-4.88 (m, 1H), 4.54-3.95 (m, 2H), 3.88-3.40 (m, 3H), 2.48-2.10 (m, 3H), 1.81-1.66 (m, 1H), 1.47 (d, *J* = 9.6 Hz, 9H). LCMS: (ES, m/z): 565.20 $[M+H]^+$

Compound **8** (Ibrutinib-phenyl-alkyne)

phenyl (2E)-4-[(3R)-3-[4-amino-3-[4-(3-ethynylphenoxy)phenyl]pyrazolo[3,4-d]pyrimidin-1-yl]piperidin-1-yl]-4-oxobut-2-enoate

To a stirred mixture of 3-[4-(3-ethynylphenoxy)phenyl]-1-[(3R)-piperidin-3-yl]pyrazolo[3,4-d]pyrimidin-4-amine (**10**, 500 mg, 1.21 mmol, 1.00 equiv) and (2E)-4-oxo-4-phenoxybut-2-enoic acid (187 mg, 0.97 mmol, 1.00 equiv) in DMF (4 mL) were added T3P (930 mg, 1.46 mmol, 1.50 equiv, 50%) and DIEA (378 mg, 2.92 mmol, 3.00 equiv). The resulting mixture was stirred for 30 min at 25 °C under nitrogen atmosphere. The mixture was poured into water (90 mL), extracted with EtOAc (90 mL). The combined organic layers were washed with brine (100 mL), dried over anhydrous Na2SO4. After filtration, the filtrate was concentrated under reduced pressure. The crude product was purified by Prep-HPLC with the following conditions: Column, XBridge Shield RP18 OBD Column, 30x150 mm; mobile phase, water (10 mmol/L NH4HCO3+0.1%NH3.H2O) and ACN (35% PhaseB up to 55% in 10 min); Detector, UV&254/220 nm.The product fraction was lyophilized to afford phenyl (2E)-4-[(3R)-3-[4-amino-3-[4-(3-ethynylphenoxy)phenyl]pyrazolo[3,4-d]pyrimidin-1-yl]piperidin-1-yl]-4-oxobut-2-enoate (76.8mg,14.62%) as a white solid. ^{1}H-NMR (400 MHz, Methanol-d_4) δ (ppm): 8.14 (s, 1H), 7.65-7.60 (m, 3H), 7.38-7.24 (m, 3H), 7.19-7.14 (m, 2H), 7.09-7.05 (m, 4H), 7.01-6.97 (m, 2H), 6.74-6.47 (m, 1H), 4.86-4.81 (m, 1H), 4.48-4.95 (m, 2H), 3.76-3.58 (m, 2H), 3.43 (s, 1H), 2.46-2.24 (m, 1H), 2.20-2.05 (m, 2H), 1.76-1.58 (m, 1H). LCMS: (ES, m/z): 585.20 $[M+H]^+$